This is a peer-reviewed, accepted author manuscript of the following conference paper: Brough, E., Nash, D., Kazemi Amiri, A. M., Couturier , P., & Reis , V. L. (2023). Development of a test rig for improved estimation of structural damping of wind turbine composite materials. In Proceedings of ASME 2023 Aerospace Structures, Structural Dynamics, and Materials Conference, SSDM 2023 Article V001T01A026. ASME. https://doi.org/10.1115/SSDM2023-108462

Proceedings of the SSDM 2023
ASME Aerospace Structures, Structural Dynamics, and Materials Conference
SSDM2023
June 19-23, 2023, Westin San Diego Bayview, San Diego, CA

SSDM-108462

DEVELOPMENT OF A TEST RIG FOR IMPROVED ESTIMATION OF STRUCTURAL DAMPING OF WIND TURBINE COMPOSITE MATERIALS

Euan Brough[1], David Nash[1], Abbas Mehrad Kazemi Amiri[1], Philippe Couturier[2], Vitor Luiz Reis[2]

[1]University of Strathclyde, Glasgow
[2]Siemens Gamesa Renewable Energy

ABSTRACT

Material damping affects the vibrational response of composite wind turbine blades, which in turn has an impact on the structural stability and fatigue life of the entire system. Understanding material-level structural damping is crucial for improving the performance and reliability of wind turbines. The present work aims to develop an increased understanding of material-level structural damping and focuses on the development of a rig to reliably quantify energy dissipation properties of candidate wind turbine materials. The novel test rig employs Experimental Modal Analysis (EMA) in a vacuum to improve experimental structural damping characterization of high-modulus materials. The test rig allows for a non-constrained, free-free suspension of a sample which minimizes energy loss mechanisms that can lead to unrepresentative results. Sample excitation methods were also compared, and an automated excitation method was devised. The capabilities of the test rig are presented by the damping extraction of aluminum specimens. The results presented also quantify the component of aerodynamic damping present by comparing EMA with and without the presence of air, for several tests, allowing for the characterization of structural damping.

Keywords: Structural Damping, Dynamic Mechanical Analysis (DMA), Experimental Modal Analysis (EMA)

NOMENCLATURE

DMA	Dynamic Mechanical Analysis
EMA	Experimental Modal Analysis
FRF	Frequency Response Function
pLSCF	Poly-Reference Least Squares Complex Frequency
SGRE	Siemens Gamesa Renewable Energy
UD	Unidirectional
WT	Wind Turbine

1. INTRODUCTION

Offshore wind energy business has grown significantly in recent years, due in part to the increasing demand for renewable energy sources[1]. As concerns about climate change have grown, governments and businesses have recognized the importance of transitioning to cleaner, more sustainable forms of energy. Offshore wind energy has the potential to play a significant role in meeting this demand, as it is a clean, reliable, and abundant source of electricity. The growth of the offshore wind energy sector has also been driven by advances in technology, which have made it easier and more cost-effective to build and operate wind turbines in offshore locations. As technology continues to improve, it is expected that onshore and more specifically offshore wind energy will play an increasingly significant role in the global energy mix. One of the key challenges in offshore wind energy is the design of wind turbine blades. The blades are subjected to a range of forces, including wind loads, gravitational loads, and inertial loads. To maximize the efficiency of the turbine, it is important to design the blades so that they can withstand these loads without failing and understand the dynamic behavior of the system.

Damping is a crucial factor to consider in the design of structures and mechanical systems, as it can affect the stability, efficiency, and overall performance. [2]. Several factors can contribute to the damping of a wind turbine blade and are discussed within this paper. There are various different types of damping, but those of relevance within this study are structural damping and aerodynamic damping. If the blade has too little damping, it can vibrate excessively, leading to fatigue and a reduction of the lifetime of the blade of alternatively, increased maintenance costs. It is therefore important to be able to precisely quantify the damping of materials used in wind turbine blades, which will allow for a better consideration of this effect in future blade designs.

The development of a novel experimental analysis test rig for the improved characterization of structural damping of selected materials is presented herein. The main goal of the research is to understand material damping and address the limitations and shortcomings of current experimental methods for its evaluation, specifically in composite materials and materials with high elastic moduli. This goal led to the development of an improved experimental methodology for characterizing material damping to better understand the damping behavior of materials and to optimize the design of structures and mechanical systems. As such, a state-of-the-art review of relevant experimental methods for characterizing material damping is presented and points to potential avenues for improving structural damping characterization. 2 The limitations and shortcomings of current methods are also discussed. 3In addition, the design and manufacture of the updated EMA test rig is described, detailing the various components of the test rig, including the design and construction of the vacuum chamber, the selection and placement of sensors and actuators, and the development of the control and data acquisition system. 4 Finally, preliminary results are presented, comparing the effect of testing in vacuum vs air with some helpful5 conclusions on the development and success of the experimental test rig is also provided.

2. Background approaches and rationale

Within this study, the quantification of structural damping of materials used within wind turbine blades was the principal focus, where structural damping refers to the dissipation of energy in a structure. Characterizing the structural damping within wind turbine applications is important, especially due to the edgewise vibrations as there is very little aerodynamic damping in this mode [3]. By better understanding the damping of materials used within blades, such as Siemens Gamesa Renewable Energy's (SGRE) SWT-3.6-107 wind turbine, the industry may improve their models for the dynamic models of these structures. As such, the materials that are initially of interest for experimentation within the developed test rig include UD carbon composites, UD glass composites, and aluminum.

Structural damping, which is a source of energy dissipation, is a result of internal mechanisms such as friction that leads to the loss of vibration energy. It is an important consideration in the design and analysis of structures, as it affects the dynamic response of the structure to loads, including the response amplitude to which the damage is directly proportionate. Damping is a property dependent on many factors, including the geometry of the structure, material, connections and joints, temperature, frequency, stress, and strain [4], [5]. Temperature can also affect the internal friction within a material altering the energy dissipation within a structure. Generally, increasing the temperature of a composite will lead to an increase in damping due to the softening of the matrix material [4]. The frequency of a system can also affect damping, as some damping mechanisms, such as internal friction, are frequency dependent.

Currently, there are several experimental methods used in industry for the quantification of damping within materials. It is important to understand why there is still difficulty in producing damping values, with high confidence and therefore the two common industrial approaches of DMA and EMA are reviewed herein [5].

Dynamic Mechanical Analysis (DMA) is a technique used to study the mechanical properties of materials, such as viscoelasticity, over a range of temperatures and frequencies [6]. DMA involves applying a small amplitude oscillatory stress or strain to a material and measuring its resulting mechanical response. The resulting loss modulus quantifies the damping behavior that would traditionally help quantify the material damping for a given sample. The literature has reported that DMA may not be the optimal solution for evaluating structural damping in wind turbine blade composites as concerns have been raised regarding the use of composite materials and materials with elastic moduli greater than 100 GPa. These high moduli can result in large errors in the measured damping properties [7]. To address this issue, a three-point bend mode is often employed in industrial DMA machines [6], [8], [9]. However, this mode introduces shear effects which can lead to overestimations of the damping properties [4]. Additionally, inaccuracies can also occur due to boundary conditions, as frictional effects are present at the support locations [10]. These may be reduced by minimizing the contact regions of the samples; however, this is yet to be validated. Therefore, it can be concluded that DMA results can have a measure of uncertainty and require further validation for evaluating damping properties in composite materials and especially those materials with high elastic moduli.

EMA is another prominent method used to determine the structural damping of selected materials. EMA is a technique used for determining the dynamic characteristics of a structure, such as natural frequencies, mode shapes, and damping ratios, by measuring its response to an applied excitation. This is accomplished by using sensors, such as accelerometers, to measure the response of a structure, and data acquisition and analysis software to extract modal parameters from the measured data. EMA also has its shortcomings when considering its application for the determination of structural damping. It was found that the boundary conditions, such as a fixed support, implemented in some testing setups could be attributed to additional energy loss from the system, thereby affecting the resulting damping results of the experiment [11]. A fixed boundary condition, as seen within the logarithmic decrement method, is an example of this. Therefore, a free-free suspension mechanism mounted at nodal lines, for each investigated mode, is preferred [11]. It was also identified that the post-processing methodology could also impact the accuracy of the resulting damping component [12]. It has also been noted that non-contact methods for excitation, such as the use of a loudspeaker, are

preferred, however, this was not an option for use in all environmental conditions that are of interest and are therefore may not be possible for all analyses [12], [13]. In addition to this non-contact methods for data acquisition would also be advantageous, however, the equipment required for this is not currently available.

Based on a thorough review of the literature, it was determined that the current methods for quantifying structural damping in materials had significant limitations, particularly in the case of composite materials and those with high elastic moduli. As a result, a new methodology for conducting Experimental Modal Analysis (EMA) was proposed, which included the design and development of a novel experimental test rig. This updated approach aimed to overcome the shortcomings of previous methods and provide more accurate and reliable data on the damping properties of the materials being studied.

3. Development of EMA Test Rig – Test Methodology

This work aims to improve the experimental characterization of structural damping within selected materials through the development of a new experimental methodology. An EMA test rig was developed at the University of Strathclyde in Glasgow for the testing of medium-scale samples, with a focus on materials used in wind turbine blades. The main goal of the experiment is to quantify modal damping at the first mode of selected materials, where the modal frequency being tested is in the same range the frequencies observed in operational wind turbine blades. In addition, the EMA rig also aims to quantify the component of aerodynamic damping, which has previously been considered to be insignificant. This new test methodology using the EMA rig was developed to address the shortcomings identified in previous methods and produce more representative results.

3.1 Requirements

The development of a novel test rig for conducting EMA to improve structural damping characterization required the definition of specific requirements for the rig. The rig aimed to serve as a versatile tool for evaluating the damping characteristics of various materials and environmental conditions, which are both critical factors affecting material damping. To achieve this, a set of design considerations were established and used as guidelines throughout the development process. These design considerations are outlined in Table 1 below.

Variable	**Requirement**
Material Compatibility	Any
Boundary Conditions	Free-Free
Vacuum Requirement	-0.9 bar (minimum)
Frequency Range	0-10 Hz
Vacuum Pumps	1/2
Excitation Method	Modal Hammer
Hammer Strike Force Range	20-100 N
Ease of use	Modular Design

TABLE 1: Design Considerations

The design considerations shown above were carefully considered when developing the novel test rig for conducting EMA. The free-free boundary condition and the use of a vacuum chamber were crucial in ensuring that the test rig would be able to accurately capture the damping characteristics of various materials and environmental conditions, without additional losses being present. The specified frequency range of interest and the use of a modal hammer excitation method were also important factors in the design of the test rig. In addition, the first flexural mode has been identified as the main interest, which is generally in the range of 0.2 – 1 Hz. Additionally, the requirement for a modular and easily disassembled equipment setup was considered to facilitate the testing of multiple samples. Overall, these design considerations have been essential in ensuring that the test rig can provide accurate and reliable results for evaluating structural damping in medium-scale samples.

3.2 Testing Frame & Suspension Mechanism

In the development of an improved EMA test methodology, it was essential to consider the suspension mechanism used to support the sample being tested. Research in the field has established that through contact mechanisms, energy can be lost from the system, which would result in inaccurately high damping values. To minimize this effect, it was determined that a free-free suspension mechanism would be the most suitable solution.

To achieve this, a modular frame was designed and constructed using aluminum profiles, as depicted in Figure 1. This frame was designed to be rigidly attached to a fixed structure to eliminate the influence of external vibrations on the test results. The frame's central spars on the top face could be positioned in various locations along the top surface to account for samples of up to 2m in length, with a maximum width of 0.25m accommodating a sample of 2m x 0.2m x 0.05m.

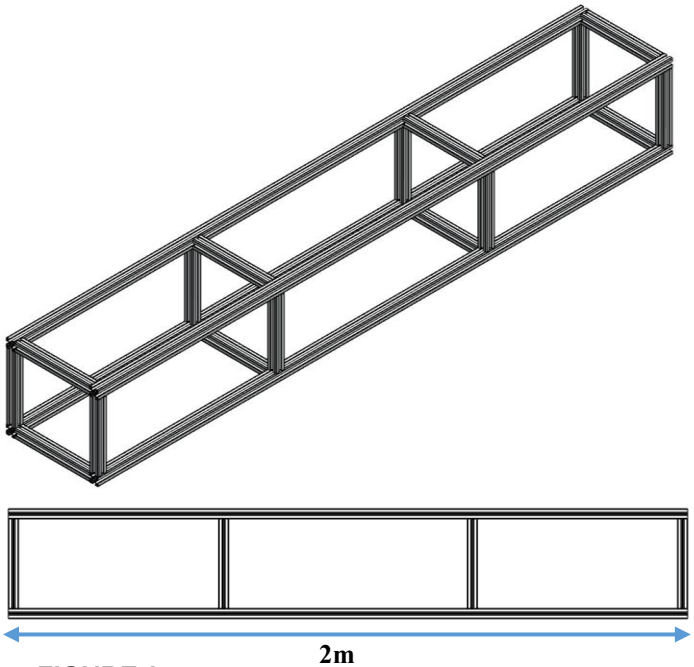

FIGURE 1: Modular Frame

The modular frame, of dimensions: 2.06 m x 0.32 m x 0.29 m, allows for a sample of up to 2m in length to be tested with EMA. The frame allows the suspension points of the sample to be selected and acts as a mount for the sample's excitation method. The frame is also to be fixed to a solid table mounted on a concrete floor to reduce the effect of any external vibration. This design is based on a dual-suspension free-free mechanism as the primary test mode, where the sample is positioned in a side-on orientation. This allows for flexibility and adaptability in testing different samples of different dimensions.

ANSYS finite element software was used to analyze the natural frequencies and mode shapes of each sample under examination in this study. The first flexural mode of the sample is of particular interest and is illustrated in Figure 2. This visual representation of the deformation of the sample at that specific frequency helps to identify the nodal and anti-nodal regions, which are the regions of minimum and maximum deformation, respectively.

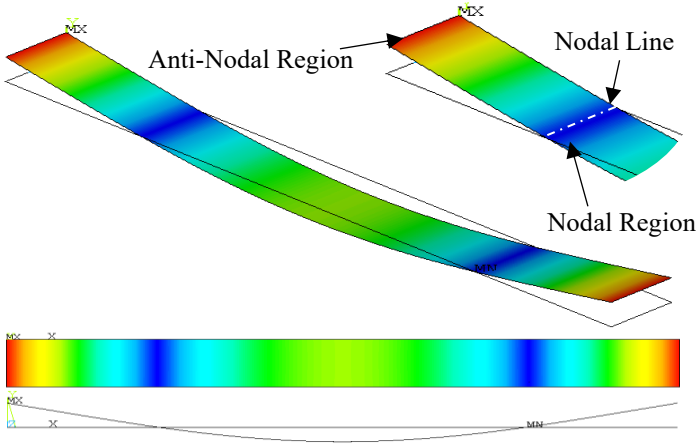

FIGURE 2: First resonant mode shape of Aluminum material of dimension 2000 x 200 x 6 mm

The diagram above displays the displacement of the beam, in its first flexural mode. The areas in dark blue, labeled as the nodal region are the areas of lowest displacement. This scale slides to warmer colors as the displacement increases with red being the areas of maximum displacement, labeled as the anti-nodal location. The nodal locations or lines are of particular interest for the suspension of the samples, as suspending the samples at these locations will have the least impact on the vibrational response of the sample around its first natural frequency. This process was conducted for each sample of different material and geometry, to ensure that energy loss through the material's suspension points is minimized. The results of this study show slight variation in the nodal line locations between the different materials and thicknesses used, however, all locations were recorded and used as the suspension points.

Once the location of the suspension was determined, using results from Figure 2 above, it was essential to thoroughly investigate various suspension methods. A comparative analysis was conducted using the frequency response function (FRF) produced by each method. The modal analysis results were utilized to eliminate suspension methods that did not align with expectations and certain methods were observed to introduce peaks in the FRF, which were identified and subsequently eliminated from consideration.

Through this examination, it was determined that the optimal suspension method involved the use of pins passing through the sample, in conjunction with nylon string support, as depicted in Figure 3. This method was found to provide the most stable and consistent results, with minimal impact on the sample's natural frequency and mode shape. The use of pins and string support was also found to minimize energy loss and ensure accurate data collection.

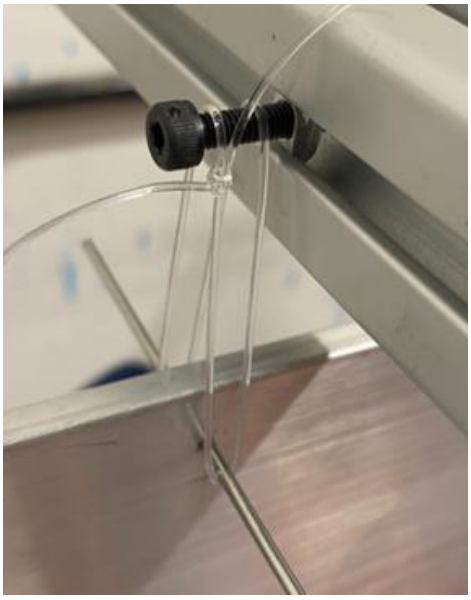

FIGURE 3: Suspension Mechanism

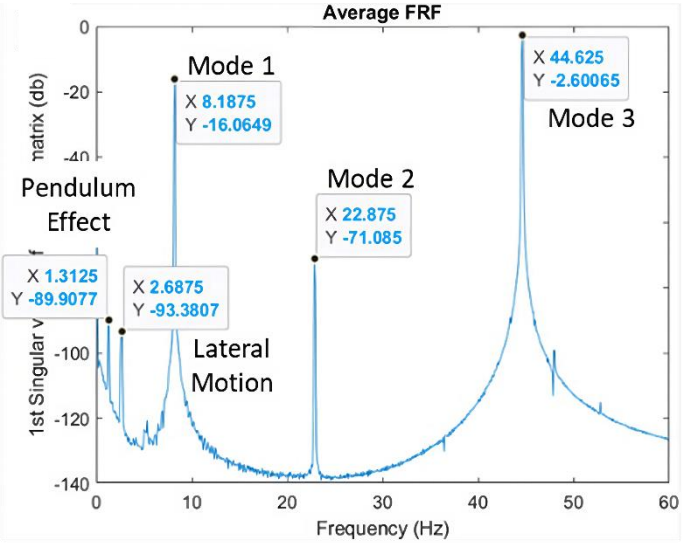

FIGURE 4: Resulting FRF

In Figure 4 above, the FRF for 0-60Hz is displayed. Within this segment, five peaks can be seen. Through testing, it was identified that the peak at 1.43 Hz was a result of the sample swaying after the strike, in the thickness direction. The second peak was also identified to be a result of rigid body motion where the sample was swaying in the length direction. The subsequent peaks were then identified as the first three modal frequencies. This was identified as an optimum setup from the study performed due to the absence of unknown peaks and FRF displaying a larger magnitude of excitation at the first modal frequency. By performing the above analysis, it was possible to create and optimize the suspension mechanism used within this test process. The frame can be placed in different environments to study the environmental effects on the damping of the same. In addition, it was also important that the frame has a minimum effect on the results. This produced a finalized suspension method as can be seen in Figure 5 below:

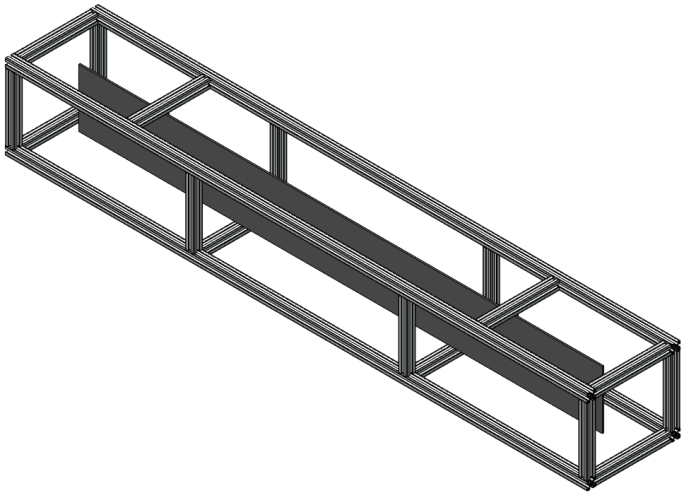

FIGURE 5: Modular Frame displaying sample suspension method

3.3 Vacuum Chamber

The purpose of the vacuum chamber is to eliminate the effect of aerodynamic damping on the results allowing the quantification of both the structural damping and aerodynamic damping components for a specific sample. By conducting the tests in a vacuum, it is possible to observe if there is an effect on damping when altering the strain rate of the sample, as aerodynamic damping contributions can be removed.

The pressure vessel was designed in accordance with PD5500 [14]. The pressure vessel was designed to meet the requirement of maintaining a complete vacuum, whilst also accommodating the modular frame and providing easy insertion and extraction of the frame and samples for each test. The vessel's dimensions were carefully chosen to meet these criteria. The vessel consists of a 2.1m length acrylic cylinder with an outer diameter of 550mm and a wall thickness of 6mm. To comply with the standard, it was necessary to add four vacuum support stiffening rings with two additional rings at each end. To increase the extent of the achievable vacuum with this apparatus, the end caps were bolted on using an external mounting mechanism. This ensured there would be no leaks through the bolting methodology itself. The design was created using SOLIDWORKS as shown in Figure 6 below:

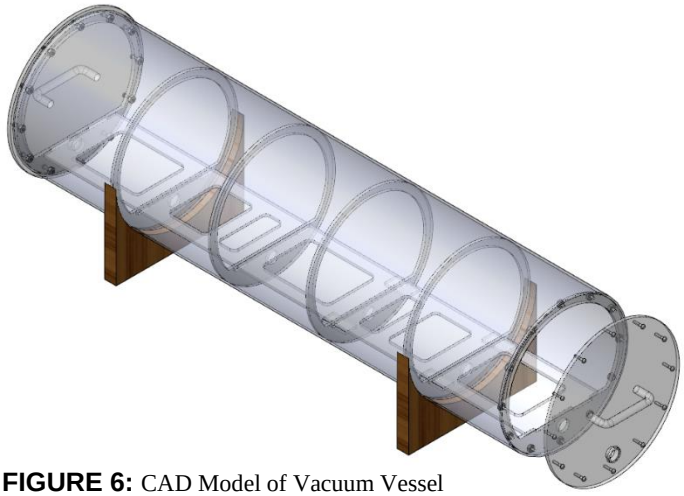

FIGURE 6: CAD Model of Vacuum Vessel

The vacuum chamber has two flat end plates made of 20mm acrylic with an outer diameter of 650mm. As seen above, the vessel is held rigidly by two saddle supports. This extended diameter allows for easy removal of the end plates in between experiments, as the chamber requires to be opened multiple times. The end plates are equipped with fittings that allow for the connection of up to two vacuum pumps via a T-connector on the first end plate, as well as two gate valves and quick disconnects that are compatible with the pumps. On the other end plate, this also uses a t-connector which features a pressure release valve and a vacuum gauge. Both end plates have cable glands installed to allow for the passage of cables and the automated hammer striker pressure system into the vacuum-controlled environment. The flat ends can be seen in Figure 7 below:

FIGURE 7: End Plate

It should be noted that in accordance with the British Standard PD5500 [14], the number of bolts installed in each end plate is 16. Inside the vacuum chamber, a flat section of acrylic is fitted to accommodate the insertion of a modular frame. The fully constructed chamber can be seen in Figure 8 below:

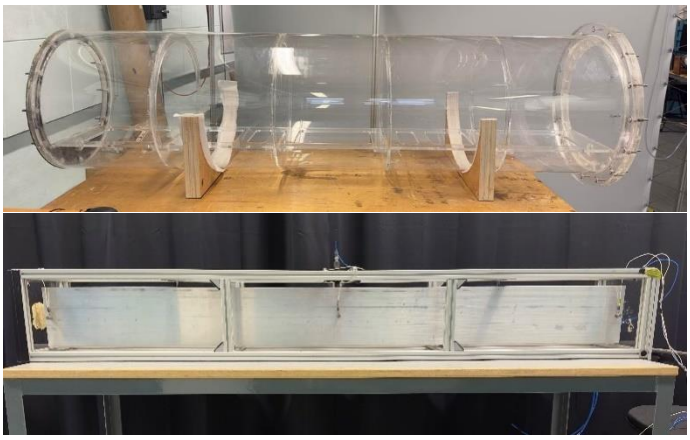

FIGURE 8: Vacuum Vessel and Modular Frame

3.4 Sample Excitation Method

To test the sample under the updated testing methodology, it must first be excited. The excitation can be performed through different methods, both contact, and non-contact methods. However, as the rig used for the testing is required to operate under vacuum conditions, it was decided that a modal hammer would be the most appropriate excitation source.

During the initial stages of bench testing, it was noticed that the consistency of the manual hammer strike (Method A) was not sufficient. While it could have been possible to sort the data according to specific force ranges, it was determined that an automated mechanism would be required for in-vacuum testing. In addition, it was also observed that the system was recording double strikes during testing. This is not acceptable as it can lead to inaccuracies in the results and compromise the integrity of the testing methodology. This prompted an investigation to be conducted where alternative automated striking technologies were considered. Two alternative striking methodologies were then created and compared against Method A (Manual Strike). Method B, where the hammer is swung forward by an extending solenoid, and Method C, where a pneumatic system was used to strike the sample via the modal hammer. These alternatives can be seen in Figure 9 below:

FIGURE 9: Method B & Method C respectively

These three methods were then compared against each other and evaluated based on their consistency and the striking force they were able to produce. A target of 60N was set and the results can be seen displayed in Figure 10 below:

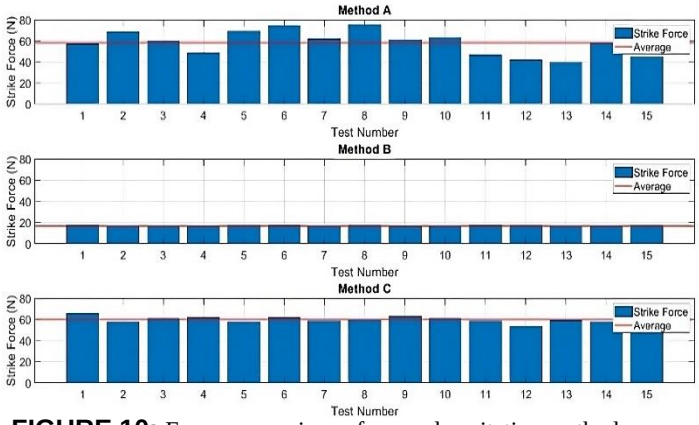

FIGURE 10: Force comparison of manual excitation method (Method A) vs. Solenoid Assisted Strike (Method B) vs. automated pneumatic striker (Method C)

From Figure 10 above, Method A can be seen to be inconsistent displaying a much larger range and standard deviation than the alternative methods. In addition, the inconsistency made it difficult to achieve the desired 60N average. Due to these limitations, Method A was removed from the contention for the striking mechanism. Both Method B & Method C can be seen to be much more consistent, however, the magnitude of Method B is not able to achieve the strike force desired. From this comparison, it was decided that Method C was the selected striking mechanism. This schematic and photo of the selected striking system was shown in the diagram in Figure 11.

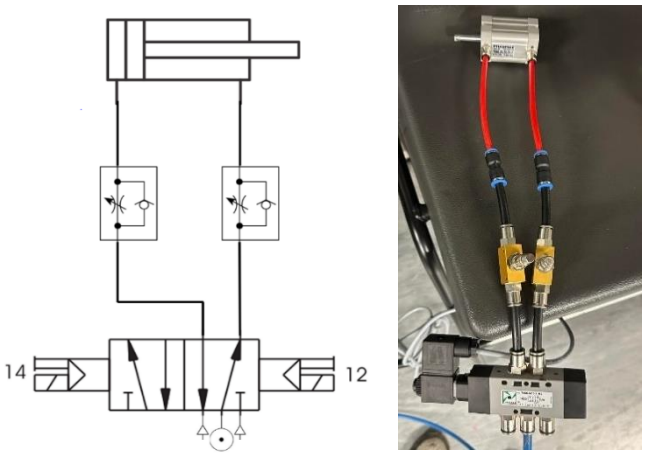

FIGURE 11: Pneumatic Actuation Device Outline (Method C)

As shown in the system diagram, a 5/2 valve is connected to an inlet air supply of 8 bar and the two airlines. These lines are equipped with single-direction restrictor valves, which enable precise adjustment of the force delivered by the modal hammer. The air flows through the restrictor valves and into the piston actuator. The direction of the piston's actuation is determined by the direction of airflow, which is controlled by the state of the solenoid in the 5/2 valve.

The final objective of the strike mechanism design required the device to ensure no double strikes were occurring, as this phenomenon should be avoided [15]. To prevent multiple strikes a control system was required to time the piston extensions. To produce a short pulse to the solenoid, the timing of the pulse was modified by using a 555-timer circuit configured to produce a single pulse signal of a selected period. This pulse controls a transistor that switches through 24V to a solenoid and creates the required piston pulse. This mechanism, upon tuning, effectively eliminated the occurrence of double strikes in this mechanism.

The pneumatic system is designed to indirectly excite the sample by striking the back side of the modal hammer. The modal hammer is mounted in a way that allows it to swing toward the sample and strike it at its midpoint. This configuration ensures that the pneumatic system does not come into direct contact with the sample and is designed so the piston actuator disconnects with the modal hammer before the strike occurs. This mechanism can be seen in Figure 12 below:

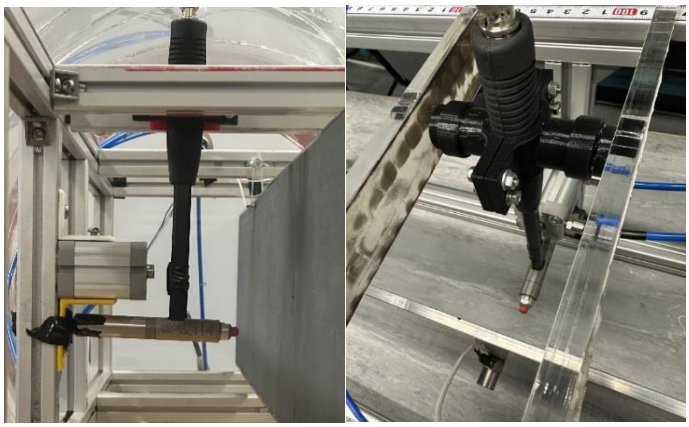

FIGURE 12: Final Pneumatic Actuation Device (Method C)

As previously stated, the implementation of a pneumatic device was chosen for its ability to generate increased force and consistent strikes compared to alternative methods. To confirm these capabilities, a series of tests were conducted to determine the device's ability to achieve a range of target forces. The restrictor valve was utilized to fine-tune the system and achieve the desired forces whilst ensuring no double strikes were occurring. Once the configuration was confirmed, 15 strikes were performed at each target force are presented in Table 2 below:

Target Force (N)	Average Force (N)	Error (%)	Standard Deviation
30	29.10	0.97	0.28
40	40.57	1.02	0.41
50	49.70	1.34	0.67
60	60.13	0.35	0.21
70	71.54	0.92	0.66
80	79.72	0.31	0.24
90	89.85	1.14	1.02
100	98.70	2.42	2.38
110	109.32	3.58	3.91

TABLE 2: Target Force vs Actual Force Table

The results of the testing indicate that the accuracy and consistency of the strike force using the automated pneumatic striker were satisfactory. As previously mentioned, increasing the inlet air pressure to 10 bar for this setup may yield higher forces, however, the laboratory where the experiment is being conducted has an inlet pressure limitation of 8 bar. Therefore, higher air pressures cannot be achieved in this current setting.

As a result of the testing conducted, the new automated striker mechanism was identified as being suitable for use. This method has been found to be consistent and capable of achieving a wide range of forces, which is essential for the test rig. Additionally, this method enables the use of an industrial modal hammer equipped with a force cell, which was validated to be reliable.

3.5 Data Acquisition

Data acquisition is crucial for capturing the response of the sample to the stimuli presented by the new automated modal hammer. In this section, the software and hardware used for this process will be discussed in detail and a list of the components used will be provided. The selection of these systems is paramount as the incorrect hardware may interfere with the results, whilst the data acquisition system must be setup in a way that record and process the data optimally.

The hardware used for data acquisition includes a compact data acquisition device (DAQ), three accelerometers, and a modal hammer. The three accelerometers are connected to the DAQ via 5m low-noise 10-32-BNC wires, while the modal

hammer was connected with a 20-ft low-noise BNC-BNC cable. The DAQ is connected to a computer that is responsible for recording the data via an RJ45 ethernet cable. Table 3 below lists the hardware used in the process:

Component	Model	Quantity
cDAQ	NI 9189	1
DAQ modules	NI 9234	1
Accelerometers	PCB 353B03	3
Modal Hammer	PCB 086C03	1
Accelerometer Cables	PCB 003C20	3
Modal Hammer Cable	PCB 003D20	1
Computer with Ethernet Port	Any	1

TABLE 3: Data acquisition hardware

It is important to note that the location of the accelerometers is crucial. As previously discussed in the suspension mechanism section of the finite element analysis, the nodal and anti-nodal locations were identified. The suspension mechanism utilizes the nodal line to minimize the effect on the results. However, to record the best data, three accelerometers were placed at the anti-nodal location. Two accelerometers were placed at either end of the sample, in the middle of the beam, on the opposite side of the modal hammer. These are the areas of greatest deformation as seen in the modal analysis. An additional accelerometer was placed in the middle of the beam, on the opposite side of the strike location. This provides another data point and allows for clear visualization of the mode shape in the post-processing stage. This setup can be seen in Figure 13 below compared to the FE results.

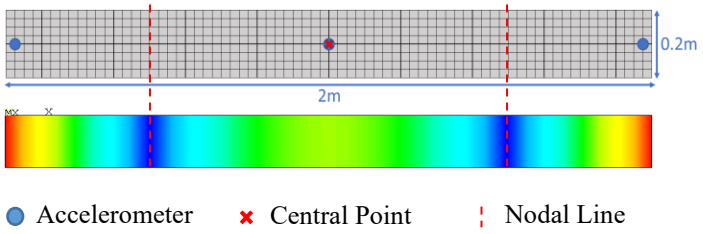

FIGURE 13: Accelerometer locations

To validate the location of accelerometers in relation to the first mode of deformation in the samples, the previously conducted FE analysis was once again viewed. The colors displayed here have the same definitions as defined in Figure 2 where the cooler blue colors represent low displacement, and the warmer red/yellow colors represent larger displacements. The images above show the correlation between the anti-nodal locations and the locations of the accelerometers. To check this expectation was correct multiple strikes of the same magnitude were performed while the accelerometers were moved over the length of the beam. The results from this study showed the area of greatest acceleration was in the anti-nodal regions. The final hardware setup can be seen in Figure 14 below.

3.6 Post-Processing

In addition to the hardware requirements, the software for data acquisition cannot be overlooked. The software used for this study is a combination of MATLAB, in collaboration with the NI plugin. This allowed for the accelerometer's recorded sensitivity to be set, as well as the sampling frequency and channel types to be labeled. Additionally, it provided good integration with the data post-processing method. This software allows for real-time data acquisition and visualization, as well as the ability to perform advanced post-processing and analysis on the collected data.

The selected post-processing tool is an industrial software toolkit, MACEC, developed by KU Leuven [16], is a powerful tool for modal analysis of structures, specifically designed for extracting modal characteristics such as eigenfrequencies, damping ratios, and mode shapes from measured vibration data. The toolbox provides extensive functionalities for data visualization and processing, system model identification, and determination of modal characteristics. In this study, the toolbox was utilized to process the data collected during the testing of the samples and extract important modal characteristics. The force data and acceleration data could be set respectively from the data input. The data was decimated by a factor of 10. A nodal model was created whereby the force applied and acceleration can be

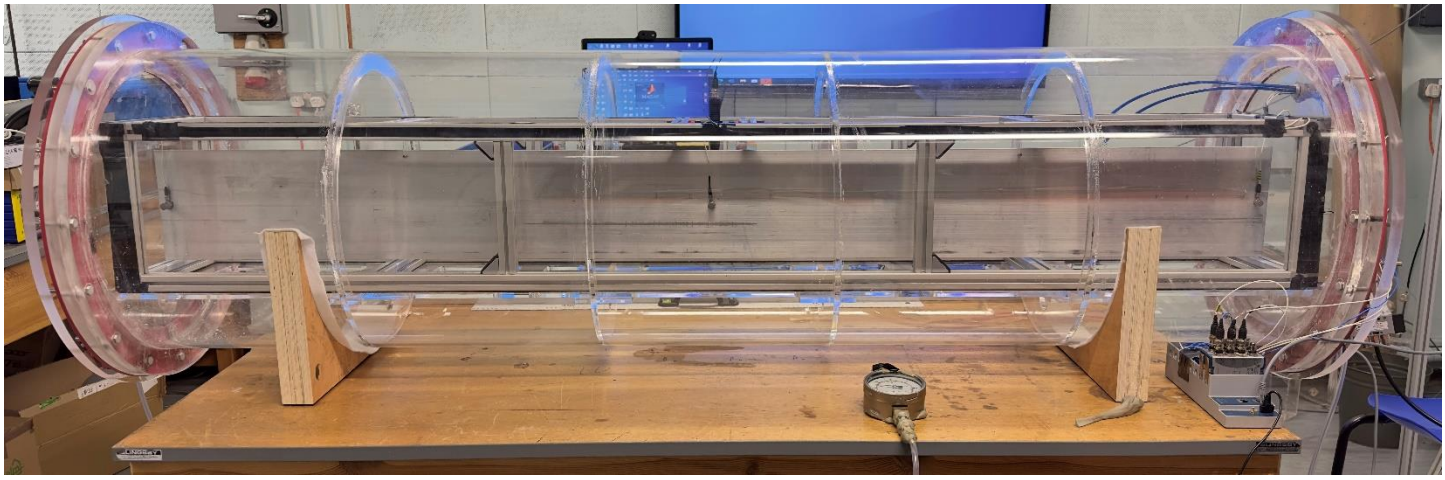

FIGURE 14: Full construction of experimental test

applied to the allocated nodes. This model can be seen below in Figure 15:

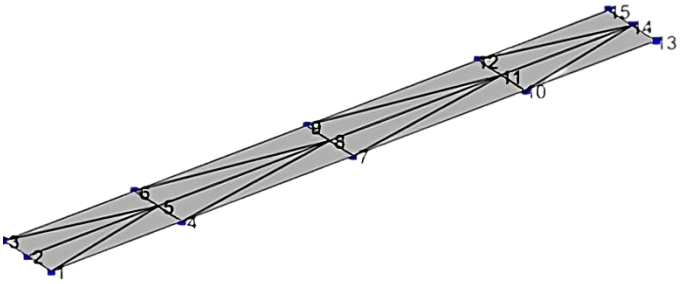

FIGURE 15: MACEC nodal surface model

From the diagram above, nodes 2, 8, and 14 were the locations of the accelerometer, with the force cell reading being located at node 8. This information was then used to evaluate the damping properties of the aluminum and compare them to the samples of aluminum, which served as a control. The built-in pLSCF was used and the stabilization diagram was used to identify a stable mode at the first modal frequency for the extraction of the structural damping.

4 RESULTS AND DISCUSSION

Within this section, some early results will be presented which should display the potential of this newly developed test rig. A comparative analysis will be presented, wherein 10 experiments conducted in air will be juxtaposed against an equivalent number of experiments conducted in vacuum. Within this study, an aluminum sample was used as the main material of interest as this provided a simpler material for the commissioning of the new testing rig. This is because metals, due to their isotropic properties and available literature damping values and provides a useful point of comparison. The inclusion of an aluminum sample allows for a better understanding of the damping properties of the composite materials in relation to a more conventional, widely used material.

After the experiment was undertaken, the data was processed using the MACEC modal analysis software. An example of a data set can be seen in Figure 16 below:

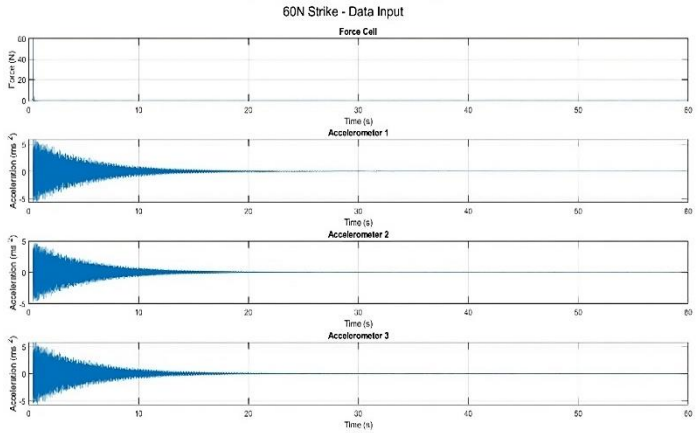

FIGURE 16: Raw Data produced

The data set above consists of a single test where the strike amplitude was set to 60N. The input signals are then processed by MACEC, implementing a decimation factor of 10. The pLSCF method was then used to produce the stabilization diagram as seen in Figure 17 below:

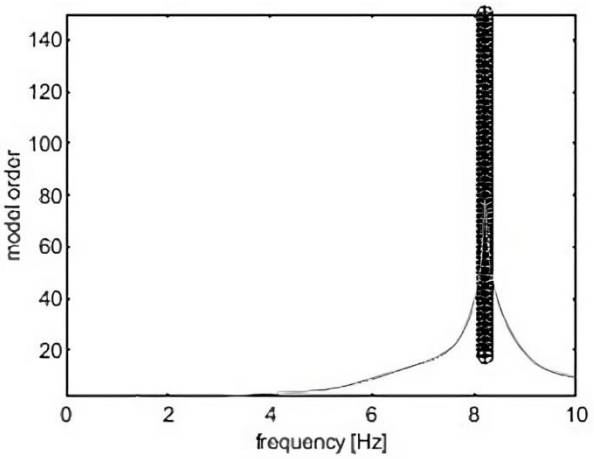

FIGURE 17: Stabilization diagram showing first mode

The stabilization diagram above allows for the identification of stable modes with natural frequencies and mode shapes being physical. This allows for these selected modes to be reliable and can be used for further analysis within this study. After identifying a stable mode, the resulting frequency and mode shape can then be compared against the results obtained by FEA. Firstly, the frequencies of the first three modes were compared against one another, as shown in Table 4. It should be noted there is no damping being modeled in the FEA and therefore there will be expected discrepancies between this, and the results obtained.

	Mode 1 (Hz)	**Mode 2 (Hz)**	**Mode 3 (Hz)**
FEA	7.7	21.4	42.0
MACEC	8.2	N/A	44.85

TABLE 4: Frequency Comparison

From the table above, it is clear to see the theoretical and experimental modal frequencies are reasonably well aligned. Mode 2 was unable to be seen in MACEC due to the free-free boundary condition applied. In addition to the modal frequency, the first mode shape can be validated. The resulting mode shape produced can be seen below, in Figure 18, and can be compared against the FE analysis in Figure 2.

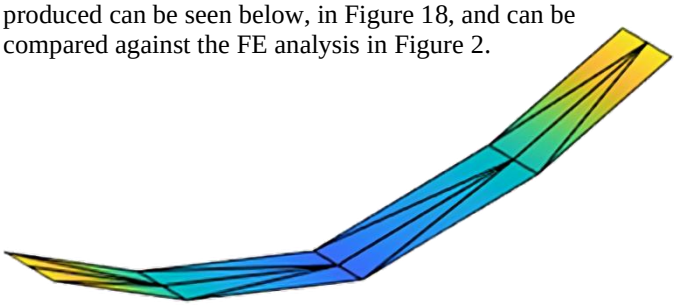

FIGURE 18: MACEC Mode Shape – Mode 1

After validation has been conducted, the resulting damping ratio for the 10 different experiments may be completed, comparing in-air and in-vacuum conditions. The results from this test can be seen in Table 5 below.

Test Number	Vacuum		Air	
	Amplitude (N)	Damping Ratio (%)	Amplitude (N)	Damping Ratio (%)
1	62.31	0.140	60.32	0.148
2	61.29	0.138	61.20	0.152
3	62.77	0.136	60.88	0.152
4	62.38	0.139	61.93	0.150
5	62.02	0.138	61.01	0.151
6	61.88	0.139	60.45	0.153
7	61.78	0.142	60.15	0.150
8	62.21	0.140	60.86	0.151
9	62.55	0.139	60.19	0.153
10	61.58	0.139	60.68	0.150
Average	**62.08**	**0.139**	**60.77**	**0.151**

TABLE 5: Damping Ratio Comparison

In Table 5 above, the damping ratio is compared within aluminum for both in-air and in-vacuum conditions subjected to the same excitation. These results show that the assumed negligible effect of aerodynamic effects may be incorrect. Upon review, it was found that the difference in damping estimation in vacuum conditions was approximately 8.5% less than that recorded in air conditions. Future work will involve the continued use of the developed EMA rig to quantify the effect of different material systems, geometries and strain rates upon the resulting structural damping component.

5 CONCLUSION

In conclusion, this study presents a new experimental test rig developed to perform EMA testing to determine the structural damping of various materials used in WT blades. The quantification of aerodynamic effects are seen to be larger than previously assumed when characterizing structural damping. In addition, through further testing it may be possible to achieve improved accuracy of structural damping and aerodynamic damping compared to other methods.

6 ACKNOWLEDGEMENTS

This work was supported by EP/S023801/1 EPSRC Centre for Doctoral Training in Wind and Marine Energy Systems and Structures, and Siemens Gamesa Renewable Energy (SGRE). I would also like to thank Lars Hedegaard for his contributions.

7 REFERENCES

[1] Global Wind Energy Council, “Wind energy in the UK: June 2021,” 2021.

[2] Anil. K. Chopra, *Dynamics of Structures: Theory and Applications to Earthquake Engineering*, vol. Fourth Edition. 2015.

[3] B. Basu, Z. Zhang, and S. R. K. Nielsen, “Damping of edgewise vibration in wind turbine blades by means of circular liquid dampers,” *Wind Energy*, vol. 19, no. 2, pp. 213–226, Feb. 2016, doi: 10.1002/we.1827.

[4] A. Treviso, B. van Genechten, D. Mundo, and M. Tournour, “Damping in composite materials: Properties and models,” *Compos B Eng*, vol. 78, pp. 144–152, Aug. 2015, doi: 10.1016/j.compositesb.2015.03.081.

[5] M. Rueppel, J. Rion, C. Dransfeld, C. Fischer, and K. Masania, “Damping of carbon fibre and flax fibre angle-ply composite laminates,” *Compos Sci Technol*, vol. 146, pp. 1–9, Jul. 2017, doi: 10.1016/j.compscitech.2017.04.011.

[6] TA, “Dynamic Mechanical Analysis - DMA Q800 - TA Instruments,” 2010.

[7] R. F. Gibson, *Principles of Composite Material Mechanics*, vol. Third Edition. 2012.

[8] M. Tehrani *et al.*, “Hybrid Carbon Fiber/Carbon Nanotube Composites for Structural Damping Applications,” *Nanotechnology*, vol. 24, no. 15, 2013, doi: 10.1088/0957-4484/24/15/155704.

[9] TA, “Dynamic Mechanical Analysis - Basic Theory & Applications Training.” 2018. [Online]. Available: http://eva.evannai.inf.uc3m.es/docencia/doctorado/cib/documentacion/OverviewIS.pdf

[10] J. Vanwalleghem, I. de Baere, M. Loccufier, and W. van Paepegem, “External damping losses in measuring the vibration damping properties in lightly damped specimens using transient time-domain methods,” *J Sound Vib*, vol. 333, no. 6, pp. 1596–1611, Mar. 2014, doi: 10.1016/j.jsv.2013.10.015.

[11] C. A. Geweth, S. K. Baydoun, F. Saati, K. Sepahvand, and S. Marburg, “Effect of boundary conditions in the experimental determination of structural damping,” *Mech Syst Signal Process*, vol. 146, Jan. 2021, doi: 10.1016/j.ymssp.2020.107052.

[12] D. A. Pereira, T. A. M. Guimarães, H. B. Resende, and D. A. Rade, “Numerical and experimental analyses of modal frequency and damping in tow-steered CFRP laminates,” *Compos Struct*, vol. 244, Jul. 2020, doi: 10.1016/j.compstruct.2020.112190.

[13] J. Vanwalleghem, I. de Baere, M. Loccufier, and W. van Paepegem, “External damping losses in measuring the vibration damping properties in lightly damped specimens using transient time-domain methods,” *J Sound Vib*, vol. 333, no. 6, pp. 1596–1611, Mar. 2014, doi: 10.1016/j.jsv.2013.10.015.

[14] Brittish Standards Instition, “PD5500 Specification for unfired, fusion welded pressure vessels,” 2021.

[15] J. Li, K. Lin, Y. Hu, Y. Yang, Y. Wang, and Z. Huang, “Multiple Impact Phenomenon in Impact Hammer Testing: Theoretical Analysis and Numerical Simulation,” *Acta Mechanica Solida Sinica*, vol. 34, no. 6, pp. 830–843, Dec. 2021, doi: 10.1007/s10338-021-00248-6.

[16] B. Peeters *et al.*, “Output-only Modal Analysis: Development of a GUI for MATLAB,” 1999. [Online]. Available: https://www.researchgate.net/publication/259600743